Journal of Inorganic Biochemistry 103 (2009) 827–832

Contents lists available at ScienceDirect

Journal of Inorganic Biochemistry

journal homepage: www.elsevier.com/locate/jinorgbio

Structure-specific binding of $[Co(phen)_2(HPIP)]^{3+}$ to a DNA duplex containing sheared G:A mismatch base pairs

Huili Chen [a,*], Chunjiao Dou [a], Yanbo Wu [a], Hua Li [b], Xiaoli Xi [a], Pin Yang [a,*]

[a] Institute of Molecular Science, Key Laboratory of Chemical Biology and Molecular Engineering of Ministry of Education, Shanxi University, Wucheng Road No 92, Shanxi, Taiyuan 030006, PR China
[b] The College of Environmental Science and Resource, Shanxi University, PR China

ARTICLE INFO

Article history:
Received 8 September 2008
Received in revised form 21 February 2009
Accepted 23 February 2009
Available online 3 March 2009

Keywords:
Mismatched DNA
Cobalt(III) complex
DNA recognition
NMR
Molecular modeling

ABSTRACT

The binding of a Co(III) complex to the decanucleotide $d(CCGAATGAGG)_2$ containing two pairs of G:A mismatches was studied by 2D-NMR, UV absorption, and molecular modeling. NMR investigations indicate that racemic $[Co(phen)_2(HPIP)]Cl_3$ [HPIP = 2-(2-hydroxyphenyl) imidazo [4,5-f][1,10] phenanthroline] binds the decanucleotide by intercalation: the HPIP ligand selectively inserts between the stacked bases from the minor groove at the terminal regions and from the major groove at the sheared region. Further, molecular modeling revealed that the recognition shows strong enantioselectivity: the Λ-isomer preferentially intercalates into the T_6G_7:A_5A_4 region from the DNA major groove, while Δ-isomer favors the terminal C_1C_2:$G_{10}G_9$ region and intercalates from the minor groove. Detailed energy analysis suggests that the steric interaction, especially the electrostatic effect, is the primary determinants of the recognition event. Melting experiments indicate that binding stabilizes the DNA duplex and increases the melting temperature by 9.5 °C. The intrinsic binding constant of the complex to the mismatched duplex was determined to be $3.5 \times 105\ M^{-1}$.

1. Introduction

Nucleotide misincorporation during DNA synthesis yields non-complementary base pairs or mismatches within the DNA helix. Base pair anomalies resulting from DNA damage are generally subject to processing by mismatch repair [1]. However, the efficiency of mismatch recognition and repair depends both on the nature of the mismatch and on the flanking DNA sequences [2–12]. If uncorrected, mismatches are fixed as mutations during the subsequent round of DNA replication. Sheared side-by-side G:A pairing has a stability similar to that of a standard Watson–Crick base pair and is therefore difficult to recognize. To probe this mismatch we have developed a bulky Co(III) intercalator, $[Co(phen)_2(HPIP)]^{3+}$ [13]. The complex employs a sterically-demanding intercalating ligand which is too wide to insert into matched B-form DNA; this instead binds preferentially to mispaired sites. We previously reported the results of an initial NMR study on the interaction of the complex with $d(GCGAGC)_2$ which contains one sheared G:A mismatch; this study indicated that $[Co(phen)_2(HPIP)]^{3+}$ selectively binds to the mismatch [13].

Nevertheless, the hexamer oligonucleotide employed is too short to form an integrated helix; in addition the conformation containing the sheared G:A base pairs is a quasi-helical duplex which weakens enantiomer selectivity for DNA binding. In the present study we have used 2D-NMR, UV absorption, and molecular modeling to explore the binding of the complex to the decanucleotide $d(CCGAATGAGG)_2$ (Fig. 1) that contains two pairs of sheared G:A mismatches. We report that binding shows high enantioselectivity: Λ-$[Co(phen)_2(HPIP)]Cl_3$ intercalates from major groove adjacent to the sheared mismatches while Δ-$[Co(phen)_2(HPIP)]Cl_3$ binds from the minor groove within the terminal regions of the duplex.

2. Experimental

2.1. Materials

The oligonucleotide d(CCGAATGAGG) was purchased from GenScript Corporation, Nanjing. Oligomer single-strand concentration was calculated from high-temperature absorbance and single-strand extinction coefficient calculated as reference [14]. When duplex formed, the concentration was approximately a half of that of single-strand. The duplex was dissolved in 0.5 ml buffer containing 20 mM NaCl, 5 mM Na_2HPO4, 5 mM NaH_2PO_4 and 0.05 mM TMSP. For imino proton studies, sample was dissolved into 90% H_2O/10% D_2O. For non-exchangeable proton studies, sample was dissolved into the phosphate buffer and repeatedly lyophilized from 99.8% D_2O in a speed vacuum, and then dissolved in 0.50 ml 99.996% D_2O with the concentration 1 mM. The complex was synthesized

* Corresponding authors. Tel./fax: +86 3517011022.
E-mail addresses: hulichen@sxu.edu.cn (H. Chen), yangpin@sxu.edu.cn (P. Yang).

0162-0134/$ - see front matter © 2009 Elsevier Inc. All rights reserved.
doi:10.1016/j.jinorgbio.2009.02.006

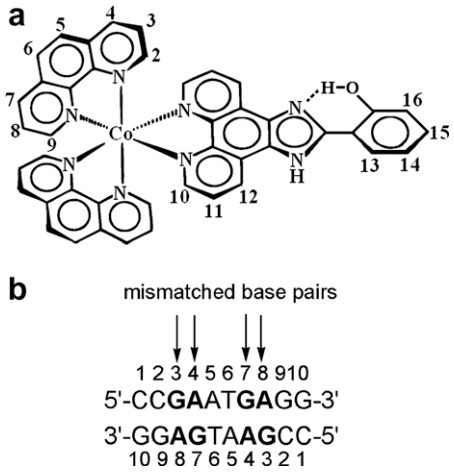

Fig. 1. (a) The structure of $[Co(phen)_2(HPIP)]^{3+}$ with atomic numbering and (b) the DNA sequence used in this work.

as previously reported [15]. Stock solution of the complex was prepared in D_2O (unbuffered) and added to the decanucleotide in 10 μl aliquots until a metal complex-to-duplex ratio (R) of 1 was achieved. The final duplex concentration was approximately 0.98 mM.

Absorbance vs. temperature melting curves were measured at 260 nm on a Hewlett Packard HP-8453 chemstation spectrometer by controlling the temperature of the sample cell with a Shimadzu circulating bath, and the intrinsic binding constant K of the complex was determined according to Eq. (1) [16], through a plot of [DNA]/($\varepsilon_a - \varepsilon_f$) vs. [DNA].

$$\frac{[DNA]}{\varepsilon_a - \varepsilon_f} = \frac{[DNA]}{\varepsilon_b - \varepsilon_f} + \frac{1}{K(\varepsilon_b - \varepsilon_f)} \quad (1)$$

where [DNA] is the concentration of DNA in base pairs, ε_a, ε_f and ε_b are, respectively, the apparent extinction coefficient ($A_{obs}/[M]$), the extinction coefficient ([DNA]/[M] = 0)for free metal complex and the extinction coefficient for the metal complex in the fully bound form ([DNA]/[M] = ∞). In plots of [DNA]/($\varepsilon_a - \varepsilon_f$) vs. [DNA], K is given by the ratio of the slope to the intercept, ε_b is obtained from the slope and a measured value of ε_f.

2.2. NMR measurements

NMR measurements were made on Bruker DRX-600 spectrometers and analyzed on a silicon graphics workstation running xwinnmr. Proton chemical shifts were referenced to an internal TMSP standard.

All NMR spectra were recorded at approximately 20 °C. Spectra recorded in 90% H_2O/10% D_2O were collected using a binomial 1:3:3:1 pulse sequence for solvent suppression. Two-dimensional phase sensitive NOESY spectra in 99.996% D_2O were recorded by TPPI method, using 2048 data points in t2 (over a spectral width of 5000 Hz) for 256 t1 values with a pulse repetition delay 2 s. Suppression of the residual HDO resonance was achieved by low-power presaturation during the relaxation delay. Phase sensitive TOCSY spectra were accumulated with 2048 data points in t2 for 256 t1 values with a pulse repetition delay 2 s.

2.3. Molecular modeling

All calculations were performed on the SGI workstation with insight II 2000 software packages. The main calculating program was DISCOVER 98. Default settings for that program were used unless specified otherwise. The complex contains one Co(III) atom with an octahedral coordination structure. Extensible and systematic force field (ESFF) could deal with both oligonucleotide and metal complex simultaneously, and give out relatively more output information for analysis, so the default ESFF force field parameters were used.

Electroneutrality of each docked structure was achieved with the addition of 15 Na^+ counterions by standard procedures to balance the nine phosphate anions on each DNA side chain and the positively charged metal complex. At the beginning of optimization and energy minimization, the Steepest Descent method was used until the root mean square (RMS) deviation was less than 5.0 kcal/mol. Then it was switched to Conjugate Gradient method automatically by the DISCOVER 98 program. When the RMS deviation was less than 0.5 kcal/mol, optimization and energy minimization was stopped.

As a starting point, the metal complex was constructed in the BUILDER module and optimized in ESFF force field. The X-ray structure of sheared DNA 5′-d(CC**GA**AT**GA**GG)$_2$-3′ (Fig. 1) was downloaded from the National Center for Biotechnology Information [17]. Each isomer was docked manually into the DNA base stack, and intercalations were simulated in major groove and in minor groove, respectively. As a beginning, the HPIP plane was placed nearly parallel to the base pairs plane (perpendicular to DNA helix axis) and just out of the DNA helix. This point was regarded as the first checkpoint, and its intercalation depth was defined as 0. Then, Co(III) complex was docked into base stack until the HPIP moiety was intercalated into the base stack entirely. We selected the checkpoint for every 0.2 nm, and the corresponding intercalation depths were thus defined as 0.2, 0.4 nm, etc. Then based on the potential energy distribution, an optimal interaction model for each isomer binding to DNA could be acquired. Modeling of all systems containing DNA was carried out in aqueous solution.

3. Results and discussion

3.1. Assignment of the proton resonances of d(CCGAATGAGG)$_2$

The ^{1}H NMR resonances of the free oligonucleotide acid were assigned from a combination of NOESY and TOCSY experiments according to standard methods [18–20]. The imino resonances in the NMR spectrum of the oligonucleotide dissolved in 90% H_2O/10% D_2O were examined to determine the extent of nucleotide base pairing. The spectrum indicates that only the terminal residues failed to form stable base pairs, with four imino resonances being observed. It is therefore believed that the oligonucleotide is predominantly present as a stable duplex in our experiments. Both the imino protons at 10.40 ppm and the downfield ^{31}P resonances (0.38 ppm and 0.12 ppm) (Supplementary material Fig. S1) indicate that two pairs of sheared G:A mismatch base pairs exist within the d(CCGAATGAGG)$_2$ duplex [21–25].

Table 1
The NOE peaks between the complex and the duplex.

Δ-Isomer	Λ-Isomer
H3,8/C_2H1′ (N)	H2,9/C_2H2′ (G)
H2,9/G_3H1′ (C)	H2,9/C_2H5 (M)
H11/A_8H2″ (D)	H14/G_3H1′ (J)
H13/C_2H2′ (F)	H14/G_3H2″ (L)
H13/C_1H5 (I)	H14/G_7H2″ (K)
H14/C_2H1′ (P)	H14/A_8H2″ (Q)
G_9H8/C_1H5 (A)	H16/G_3H2″ (H)
G_9H8–C_1H2′ (E)	H11/A_4H2′ (VW)
C_1H6–C_2H5 (O)	A_4H2/G_7H1′ (S)
	A_5H8/A_4H3′ (B)

3.2. NMR analysis of $[Co(phen)_2(HPIP)]^{3+}$ binding to mismatched DNA

The resonances of the free complex were assigned based on the COSY spectrum (see Ref. [13] and Supplementary material Fig. 2S and Table S1). The resonances from the phen moiety are easily distinguished from HPIP protons by integration of the resonances. Within each ring system the resonances were then assigned to particular protons from the COSY spectrum. One set of resonances from two ancillary ligand phen moieties indicates the symmetrical structure of the complex, therefore it is not possible unambiguously to distinguish the resonances of protons 5,4,3,2 from 6,7,8,9. We assigned these protons to H5/6, H4/7, H3/8, and H2/9, respectively. H2/9 was coupled with H3/8 by vicinal $^3J_{H-H}$ 8.0 Hz while this was coupled with H4/7 by long-range $^4J_{H-H}$. In conse-

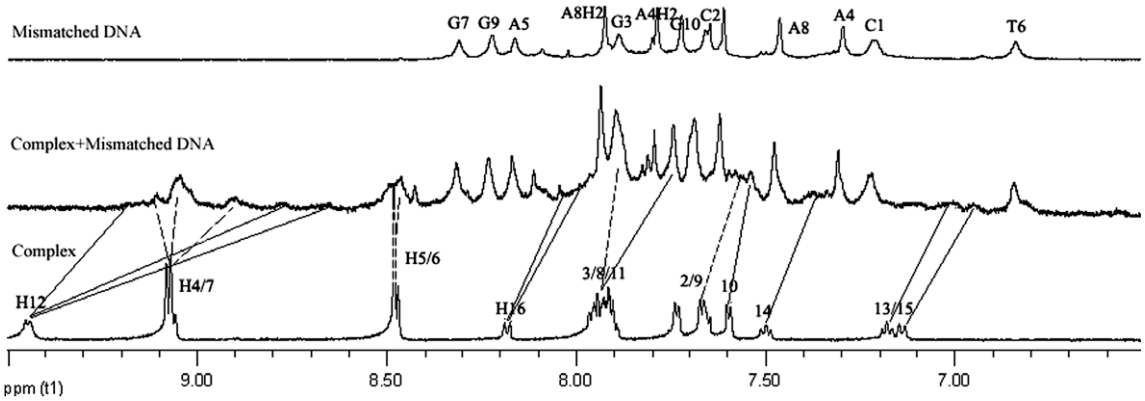

Fig. 2. 600 MHz ^{1}H NMR spectra of $[Co(phen)_2(HPIP)]^{3+}$–d(CCGAATGAGG)$_2$ at the ratio (R) of metal complex-to-duplex 1 (0.98 mM duplex) in the aromatic region.

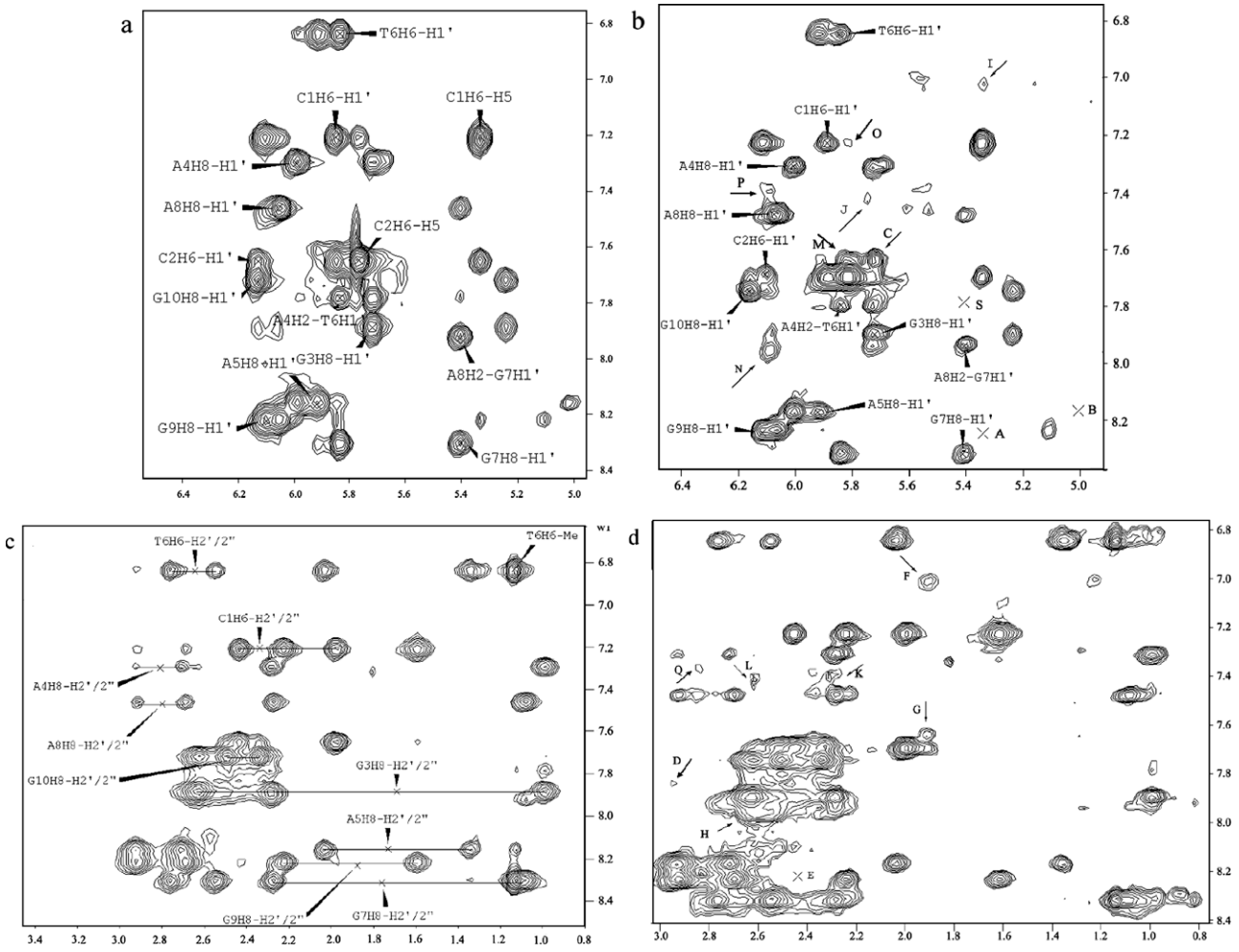

Fig. 3. Expansion of the NOESY spectrum (300 ms mixing time) of free- and $[Co(phen)_2(HPIP)]^{3+}$-bounded-d(CCGAATGAGG)$_2$ at a metal complex-to-duplex ratio of 1. (a and b) The aromatic to the sugar H1′ region of free- and complex-bounded-duplex and (c and d) the aromatic to the sugar H2′/H2″ region of free- and complex-bounded-duplex. The NOEs from the cobalt complex resonances to the decanucleotide are labeled. × indicates the disappearance of the intrastrand sequential NOEs.

quence, the coupling constant from H2/9–H3/8 was larger than that from H2/9–H4/7, and the cross-peak from H2/9–H3/8 was stronger than that from H2/9–H4/7. The resonance from H4/7 was assigned by its downfield chemical shift 9.07 ppm with respect to reference [13,26,27]; the resonance from H2/9 (7.65 ppm and 7.72 ppm) H3/8 (7.89–7.96 ppm) could also be confirmed from the COSY spectrum. H5/6 (8.48 ppm) failed to couple with other protons and showed a single peak. The resonances from HPIP were similarly assigned. The assignment for the duplex-bound complex was based on TOCSY and NOESY experiments (see Supplementary material Fig. S4) and referenced to the free complex. The resonances at approximately 8.56–8.39 ppm were assigned to H5/6 which failed to couple with other protons. H4/7 was assigned through the strong NOE between approximately 9.12–8.97 ppm and H5/6. Accordingly, the resonances from H2/9 (7.70–7.55 ppm) and H3/8 (7.94–7.84 ppm) could also be assigned by the intensities of the cross-peaks with H4/7. Similarly, the protons of HPIP within the other ring system were assigned by the combination of NOESY and TOCSY experiments. H12 (9.19 ppm and 8.80–8.63 ppm) was located at downfield and showed no NOE cross-peak with H5/6. H11 (7.91–7.81 ppm) and H10 (7.58–7.53 ppm) was assigned by their ^{3}J (8.5 Hz) and ^{4}J coupling with H12. The protons H13–H16 constitute another spin-couple system and were assigned by TOCSY. The proton sequence in chemical shift was also referenced to the previously reported hexanucleotide-bound-$[Co(phen)_2(HPIP)]^{3+}$ [13], $[Ru(phen)_2(DPPZ)]^{2+}$ [26] and $[Ru(phen)_2(DPQ)]^{2+}$ [27]. The possible chemical shift differences for intercalated ligand protons are restricted to within 0−1.6 ppm upfield from the location of the free ligand resonances [28,29].Addition of $[Co(phen)_2(HPIP)]^{3+}$ to $d(CCGAATGAGG)_2$ induced large upfield chemical shift changes for the ligand HPIP (especially H11,12,13,14,15,16), while small shifts were observed for the ancillary ligand phen (Fig. 2). This behavior is consistent with preferential oligonucleotide binding of the HPIP ligand by intercalation [30–32]. The interaction between the complex and $d(CCGAATGAGG)_2$ leads to two sets of resonances from phen and HPIP (Table 1), suggesting that there may be two binding sites. However, addition of the complex to the oligonucleotide induced only small changes in the chemical shifts of the resonances from the decanucleotide (Supplementary material Fig. S3).

A NOESY spectrum of $d(CCGAATGAGG)_2$ with added $[Co(phen)_2(HPIP)]^{3+}$ (1:1) was recorded at 20 °C with mixing time of 300 ms (Fig. 3). In addition to the expected intraduplex sequential NOEs from the oligonucleotide, a considerable number of intermolecular NOE cross-peaks between $[Co(phen)_2(HPIP)]^{3+}$ to $d(CCGAATGAGG)_2$ were observed (Fig. 3). Strong phen-to-sugar proton NOE cross-peaks, such as H3/8–C_2H1′ (N), H2/9–G_3H1′ (C), are clearly observed. Because the sugar H1′ protons are located in the decanucleotide minor groove, the NOESY data indicate that the phen ligands are bound in the minor groove. This conclusion is further supported by the observation of NOE cross-peaks between phen H2/9 and the decanucleotide H4′/H5′/5″ (protons located in the minor groove). Intermolecular NOE cross-peaks from the ligand HPIP to major groove protons are observed, such as H13–C_2H2′ and C_1H5. Importantly, some intranucleotide NOEs located in the major region were absent, including C_1H6–C_1H5 (O), G_9H8–C_1H2′ (E) and G_9H8–C_1H5 (A). The NOE data therefore indicate that the complex binds the decanucleotide by intercalation with the HPIP ligand selectively inserted from the minor groove between the stacked bases in the terminal region.

However, new NOE cross-peaks from HPIP to minor groove protons were also observed; these included H14–G_7H2″ (K), G_3H1′ (J), G_3H2″ (L), and H16–G_3H2″ (H). Concomitantly, NOEs appeared from phen H2/9 to major groove protons including C_2H2′ (G) and C_2H5 (M). These NOE cross-peaks indicated that the complex binds the decanucleotide by intercalation between the stacked bases proximal to the mismatch region, with the HPIP ligand selectively inserted from the major groove and extending into the minor groove. The disappearance of sequential intranucleotide NOEs provides further evidence; this includes A_5H8–A_4H3′ (B) and A_4H2–G_7H1′ (S).

The imino resonance spectrum in 90% H_2O/10% D_2O indicates that the double-stranded structure of the decanucleotide is maintained after $[Co(phen)_2(HPIP)]^{3+}$ binding. Moreover, the two shoulder peaks neighboring the T_6 imino resonance reveal that the region neighboring T_6 is affected by addition of the complex (Supplementary material Fig. S3).

3.3. Thermal denaturation profiles of the duplex containing two sheared G:A mismatches

Thermal denaturation profiles for the free- and metal complex-bound-duplex (3.3 μM for each strand) were measured in the same buffer as for the NMR experiment. The absorbance of the sample was monitored at 260 nm from 15 °C to 60 °C in the absence or presence of the Co(III) complex. Measurements were carried out at a complex concentration of 33 μM. The melting temperature (T_m) of the duplex was determined as the temperature crossing the melting curve at the median of two straight lines drawn for

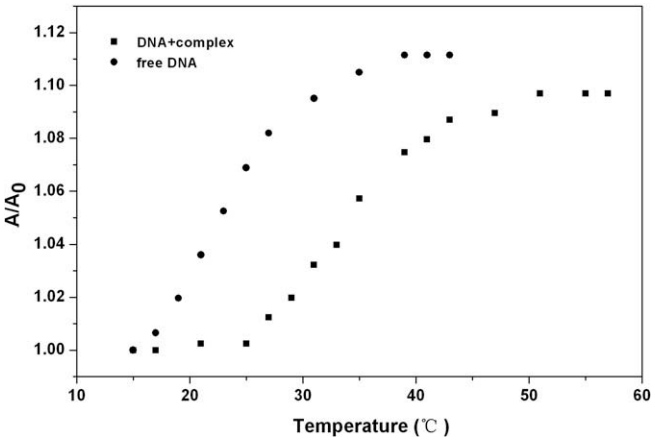

Fig. 4. Effect of the Co(III) complex on the melting temperature of $d(CCGAATGAGG)_2$ (3.3 μM) with a complex-to-duplex ratio of 10:1. $d(CCGAATGAGG)_2$ (circle) and $[Co(phen)_2(HPIP)]^{3+}$–$d(CCGAATGAGG)_2$ (square).

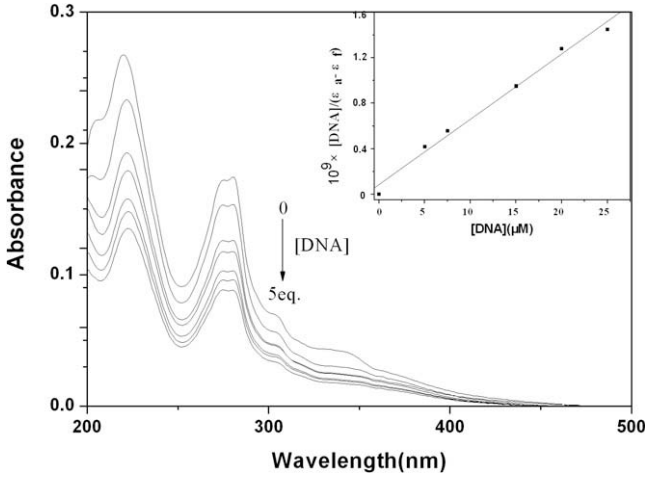

Fig. 5. Changes in the UV spectra of $[Co(phen)_2HPIP]^{3+}$ in the PBS buffer with various amounts of the mismatched oligonucleotide (0–5 equiv). [Co] = 5 μmol/L and [DNA]/[Co] = 0, 1.0, 1.5, 3.0, 4.0, and 5.0.

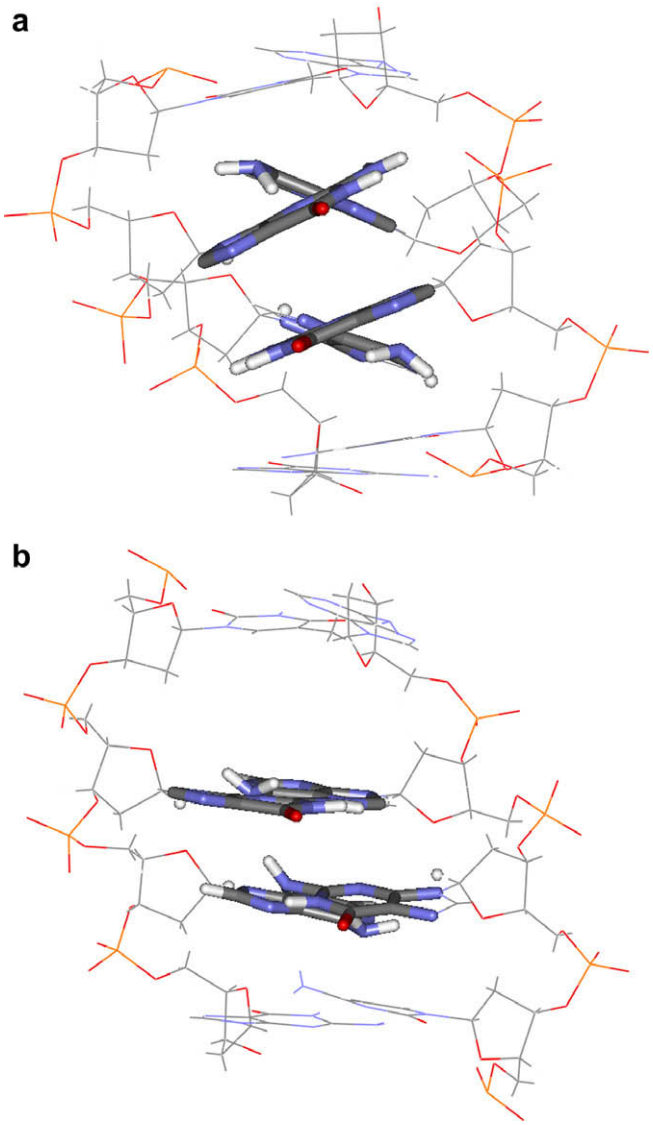

Fig. 6. The sketch map at mismatched region $d(T_6G_7A_8G_9)_2$ of the duplex (a) sheared conformation and (b) parallel conformation of mismatched base pairs after binding by Λ-isomer.

the single-strand and duplex regions in the melting curve. As shown in Fig. 4, the binding of the complex increases the T_m of $d(CCGAATGAGG)_2$ from 25 °C to 34.5 °C. The increase in T_m provides strong support for the intercalation of $[Co(phen)_2(HPIP)]^{3+}$ into the duplex, and further proves that the oligonucleotide adopts a double-stranded configuration under our experimental conditions.

3.4. Electronic absorption titration

The interaction between the complex and the mismatched oligonucleotide was investigated using absorption spectra. The electronic absorption spectra of the complex in the absence and the presence of the duplex are illustrated in Fig. 5. Addition of DNA results in a decrease in the peak intensities. Hypochromism suggested that there is a strong stacking interaction between the electronic state of the intercalated chromophore and that of the DNA bases, a general observation for the binding of intercalating molecules to DNA [33,34]. The intrinsic binding constant is $3.5 \times 10^5\ M^{-1}$ based on the hypochromism at 280 nm.

3.5. Molecular modeling

To acquire detailed binding information we carried out a computational examination of interactions between the Co(III) complex and the duplex using molecular modeling. The results of this calculation are detailed in the Supplementary material. A significant difference in calculated potential energies indicates that the Λ-isomer preferentially inserts from the major groove adjacent to the mismatches, while the Δ-isomer preferentially inserts from the minor groove within the terminal regions of the duplex. Moreover, the complex of the Λ-isomer with the duplex may be more stable than of the complex formed with the Δ-isomer. When optimal models were investigated we found that Λ-isomer has the potential to alter the conformation of the sheared DNA, converting the G_7A_8:A_4G_3 base pairs from sheared to parallel forms (Fig. 6). By combining the optimal binding models we were able to assign most of the intermolecular NOEs between the metal complex and duplex.

Molecular modeling reveals that the interaction of the Co(III) complex with the mismatched DNA shows obvious enantioselectivity for complex formation, groove-selectivity, and site-specificity for sheared DNA. This finding is consistent with our previous work [35–41] and detailed energy analysis is also consistent with

Table 2
Detailed energy distribution for interactions of Λ-isomer in DNA major groove orientation (kcal/mol).

items	Λ-Isomer in								
	C_1C_2	C_2G_3	G_3A_4	A_4A_5	A_5T_6	T_6G_7	G_7A_8	A_8Gs_9	G_9G_{10}
Total	3083	3089	3118	3067	3109	3017	3081	3139	3052
Internal	656	622	624	648	625	637	637	620	657
Non-bond	2431	2466	2494	2419	2484	2379	2444	2519	2395
VDW	−1.95	0.53	−5.99	−5.64	0.19	−3.56	6.25	2.5	−0.58
Elect	2433	2466	2500	2424	2484	2384	2438	2517	2395

Table 3
Detailed energy distribution for interactions of Δ-isomer in DNA minor groove orientation (kcal/mol).

items	Δ-isomer in								
	C_1C_2	C_2G_3	G_3A_4	A_4A_5	A_5T_6	T_6G_7	G_7A_8	A_8G_9	G_9G_{10}
Total	3042	3104	3134	3069	3060	3105	3097	3079	3133
Internal	643	632	615	647	635	648	656	666	642
Non-bond	2399	2471	2519	2421	2425	2457	2441	2413	2490
VDW	−25.4	−14.2	−4.3	−12.6	−26.63	−5.84	14.4	0.21	−21.5
Elect	2425	2486	2523	2434	2451	2463	2427	2413	2512

the results obtained. The sub-items for total energy at optimal depths in the minor groove for the Δ-isomer and those in the major groove for the Λ-isomer are depicted in Tables 2 and 3. As shown in the tables, steric (non-bond) items are more influential for DNA recognition than are the internal items as the former is of greater magnitude than the latter. For non-bond interactions the electrostatic energy is 10^2–10^3 times as large as the VDW energy, and determines the magnitude of the total energy. As shown in Table 3, when the Λ-isomer intercalates from the major groove into the T_6G_7:A_4A_5 DNA region of sheared base pairs the electrostatic energy is minimal at all interaction sites and is consistent with a well-stacked structure. On the other hand, both the internal and VDW energies are also relatively weak, revealing little bond deviation from standard values and reduced intramolecular and intermolecular steric collision.

4. Conclusions

The following conclusions may be drawn from the results reported here. First, for racemic $[Co(phen)_2\text{-HPIP}]^{3+}$–DNA interactions, selective intercalation of the metal complex into DNA was observed, with HPIP as the intercalating moiety. Second, binding shows obvious enantioselectivity, site-specificity and groove-selectivity: the Λ-isomer recognizes the mismatched region from the major groove, while the Δ-isomer recognizes the terminal region from the minor groove. Third, the steric interaction, especially the electrostatic effect, is the primary determinants of the recognition event. Fourth, the binding of the complex stabilizes the duplex conformation of the mismatched DNA.

The interactions between racemic $[Co(phen)_2HPIP]^{3+}$ and an oligonucleotide duplex were studied through NMR combined with molecular modeling. NMR investigations reveal the acting mode while molecular modeling indicates the likely sites of interaction for the different isomers. Overall, the results of this study demonstrate that the octahedral metallointercalator Λ-$[Co(phen)_2(HPIP)]^{3+}$ can recognize mismatched regions within a DNA duplex; this finding may have applications in the design of mismatch-specific chemical agents.

5. Abbreviations

phen	1,10-phenanthroline
TMSP	3-trimethylsilyl-[2,2,3,3-D4] propionate
SGI	Silicon Graphics, Inc.
NOESY	nuclear overhauser effect spectroscopy
COSY	correlated spectroscopy
TOCSY	total correlation spectroscopy
Total	total energy
VDW	van der Waals energy
Elect	electrostatic energy
non-bond	non-bond energy (the sum of the VDW and Elect) which describes the steric interactions;
internal	the internal energy which describes bond properties

Acknowledgements

The authors gratefully acknowledge the financial support of this work by the National Natural Science Foundation of China (No: 20601018) and the Shanxi Provincial Natural Science Foundation for Youth.

Appendix A. Supplementary material

The imino proton and sugar H1′ ^{1}H NMR and ^{31}P NMR spectra of the free and complex-bound-duplex. Contour plots of the TOCSY and NOESY spectrum of $d(CCGAATGAGG)^{2-}$ bounded-complex; ^{1}H NMR chemical shift data for $[Co(phen)_2(HPIP)]^{3+}$ Bound to $d(CCGAATGAGG)_2$. The data on the molecular modeling. Supplementary data associated with this article can be found, in the online version, at doi:10.1016/j.jinorgbio.2009.02.006.

References

[1] R.R. Iyer, A. Pluciennik, V. Burdett, P.L. Modrich, Chem. Rev. 106 (2006) 302–323.
[2] B. Kramer, W. Kramer, H.J. Fritz, Cell 38 (1984) 879–887.
[3] G.V. Fazakerley, E. Quignard, A. Woisard, W. Guschlbauer, G.A. van der Marel, J.H. van Boom, M. Jones, M. Radman, EMBO J. 13 (1986) 3697–3703.
[4] B.A. Jackson, V.Y. Alekseyev, J.K. Barton, Biochemistry 38 (1999) 4655–4662.
[5] B.A. Jackson, J.K. Barton, J. Am. Chem. Soc. 119 (1997) 12986–12987.
[6] B.A. Jackson, J.K. Barton, Inorg. Chem. 43 (2004) 4570–4578.
[7] B.M. Zeglis, J.K. Barton, J. Am. Chem. Soc. 128 (2006) 5654–5655.
[8] H. Junicke, J.R. Hart, J. Kisko, O. Glebov, I.R. Kirsch, J.K. Barton, PNAS 100 (2003) 3737–3742.
[9] J.R. Hart, O. Glebov, R.J. Ernst, I.R. Kirsch, J.K. Barton, PNAS 103 (2006) 15359–15363.
[10] E. Yavin, E.D.A. Stemp, V.L. O'Shea, S.S. David, J.K. Barton, PNAS 103 (2006) 3610–3614.
[11] V.C. Pierre, J.T. Kaiser, J.K. Barton, J.K. Barton, PNAS 104 (2007) 429–434.
[12] L.A. Loeb, K.R. Loeb, J.P. Anderson, PNAS 100 (2003) 776–781.
[13] H.L. Chen, P. Yang, C.X. Yuan, X.H. Pu, Eur. J. Inorg. Chem. (2005) 3141–3148.
[14] P.N. Borer, in: G.D. Fasman (Ed.), Handbook of Biochemistry and Molecular Biology: Nucleic Acids, third ed., vol. I, CRC Press, Cleveland, OH, 1975.
[15] H.L. Chen, P. Yang, Chinese J. Chem. 20 (2002) 1529–1535.
[16] J.G. Liu, B.H. Ye, H. Li, Q.X. Zhen, L.N. Ji, Y.H. Fu, J. Inorg. Biochem. 76 (1999) 265–271.
[17] <http://www.ncbi.nlm.nih.gov/Entrez>.
[18] R.M. Scheek, R. Boelens, N. Russo, J.H. van Boom, R. Kaptein, Biochemistry 23 (1984) 1371–1376.
[19] J. Feigon, W. Leupin, W.A. Denny, D.R. Kearns, Biochemistry 22 (1983) 5943–5951.
[20] D.J. Patel, L. Shapiro, D.J. Hare, Biol. Chem. 261 (1986) 1223–1229.
[21] R. Wing, H. Drew, T. Takano, C. Broka, S. Tanaka, K. Itakura, R.E. Dickerson, Nature 287 (1980) 755–758.
[22] S.H. Chou, J.W. Cheng, O.Y. Fedoroff, B.R. Reid, J. Mol. Biol. 241 (1994) 467–479.
[23] S.H. Chou, J.W. Cheng, O.Y. Fedoroff, V.P. Chuprina, B.R. Reid, J. Am. Chem. Soc. 114 (1992) 3114–3115.
[24] S.H. Chou, J.W. Cheng, B.R. Reid, J. Mol. Biol. 228 (1992) 138–155.
[25] Y. Li, G. Zon, W.D. Wilson, Proc. Natl. Acad. Sci. USA 88 (1991) 26–30.
[26] C.M. Dupureur, J.K. Barton, Inorg. Chem. 36 (1997) 33–43.
[27] J.G. Collins, A.D. Sleeman, J.R. Aldrich-Wright, I. Greguric, T.W. Hambley, Inorg. Chem. 37 (1998) 3133–3141.
[28] C. Giessner-Prettre, B. Pullman, Quart. Rev. Biophys. 20 (1987) 113–172.
[29] C. Giessner-Prettre, B. Pullman, Rev. Biophys. Res. Commun. 70 (1976) 578–586.
[30] C.M. Dupureur, J.K. Barton, J. Am. Chem. Soc. 116 (1994) 10286–10287.
[31] M. Eriksson, M. Leijon, C. Hiort, B. Norden, A. Graslund, J. Am. Chem. Soc. 114 (1992) 4933–4934.
[32] J. Feigon, W.A. Denny, W. Leupin, D.R. Kearns, J. Med. Chem. 27 (1984) 450–465.
[33] J.G. Liu, B.H. Ye, Q.L. Zhang, X.H. Zou, Q.X. Zhen, X. Tian, L.N. Ji, JBIC 5 (2000) 119–128.
[34] W.J. Mei, J. Liu, K.C. Zheng, L.J. Lin, H. Chao, A.X. Li, F.C. Yun, Liang N. Ji, Dalton Trans. (2003) 1352–1359.
[35] Z.H. Xiong, P. Yang, J. Mol. Struct. (Theochem.) 620 (2003) 129–138.
[36] Z.H. Xiong, P. Yang, Chem. J. Chinese Univ. 23 (2002) 57–63 (in Chinese).
[37] P. Yang, D.X. Han, Sci. China, Ser. B 43 (2000) 516–523.
[38] Z.H. Xiong, P. Yang, J. Mol. Struct. (Theochem.) 582 (2002) 107–117.
[39] Y.B. Wu, H.L. Chen, P. Yang, Z.H. Xiong, J. Inorg. Biochem. 99 (2005) 1126–1134.
[40] Y.B. Wu, C.P. Zhang, P. Yang, Sci. China, Ser. B 49 (2006) 2177–2185.
[41] Y.B. Wu, Z.H. Xiong, H.L. Chen, P. Yang, J. Mol. Struct. (Theochem.) 806 (2007) 247–252.